ANZIAM J. **65** (2023), 155–177
doi:10.1017/S1446181123000068

AN EXAMINATION OF THE "LANIER WING" DESIGN

Y. M. STOKES[1], W. L. SWEATMAN[2] and G. C. HOCKING[3]

(Received 1 March, 2023; accepted 10 May, 2023; first published online 21 July, 2023)

Abstract

Six patents were secured by E. H. Lanier from 1930 to 1933 for aeroplane designs that were intended to be exceptionally stable. A feature of five of these was a flow-induced "vacuum chamber" which was thought to provide superior stability and increased lift compared to typical wing designs. Initially, this chamber was in the fuselage, but later designs placed it in the wing by replacing a section of the upper skin of the wing with a series of angled slats. We report upon an investigation of the Lanier wing design using inviscid aerodynamic theory and viscous numerical simulations. This took place at the 2005 Australia–New Zealand Mathematics-in-Industry Study Group. The evidence from this investigation does not support the claims but, rather, suggests that any improvement in lift and/or stability seen in the few prototypes that were built was, most probably, due to thicker airfoils than were typical at the time.

2020 *Mathematics subject classification*: primary 76-10; secondary 76G25.

Keywords and phrases: aerodynamics, Edward H. Lanier, vacuplane, slat-wing airfoil, lift and drag.

1. Introduction

This paper concerns a problem investigated at a mathematics-in-industry study group. We start with some background on these and then move on to the investigation itself.

1.1. Mathematics-in-industry study groups Study groups with industry originated in Oxford in 1968. Subsequently, the concept has spread across the globe. The

[1]Mathematical Sciences, The University of Adelaide, South Australia, Australia;
e-mail: yvonne.stokes@adelaide.edu.au
[2]School of Mathematical and Computational Sciences, Massey University, Auckland, New Zealand;
e-mail: w.sweatman@massey.ac.nz
[3]Mathematics and Statistics, Murdoch University, Western Australia, Australia;
e-mail: g.hocking@murdoch.edu.au

year 1984 saw the commencement of the annual combined Australia–New Zealand Mathematics-in-Industry Study Group (MISG) [3, 21, 22]; 2023 will mark the 40th anniversary. During these meetings small teams of participants spend a week working on challenges brought by industry. Challenges and industries are varied. Sometimes industrial partners come back multiple times with different problems, for example, the Australian/New Zealand Steel Industry [21]. Each team reports back at the end of the week. Typically, the industries report that valuable insight was gained from the mathematical analysis of their problems. Following the study week, a written report is, usually, prepared. In recent years (since 2010), these reports have been published in the electronic supplement to the ANZIAM Journal, but they were previously collected in a proceedings. Sometimes, the work leads to further research.

A hallmark of the career of Professor Graeme Hocking is his significant support of and contributions to industry workshops, in particular in Australia, New Zealand, South Africa and Ireland. He has continuously participated in the MISG over many years. At the 2005 MISG held at the Albany campus of Massey University, New Zealand, the authors of this paper had the pleasure of jointly moderating an investigation of ideas described by Edward H. Lanier in a number of patents [13–18] on design of an aeroplane wing; this was a somewhat unusual problem for an MISG, brought by a small company, BackYard TEch, interested in establishing the veracity of the ideas. Noting that the report appeared only in a not readily accessible MISG proceedings [10], that a brief uninformative reference to the study-group work has been made subsequently [11], but without reference to the report itself, and that simplified models can provide valuable insight to complex problems such as flight, we here present a revised form of the MISG report.

1.2. The problem Edward H. Lanier obtained a series of six United States patents between 1930 and 1933 on aircraft design [13–18]. His overall aim was to produce an exceptionally stable aeroplane that would both fly normally and recover from undesirable attitudes without pilot intervention. One specific idea Lanier included in his patents is the creation of a vacuum cavity in the aircraft wing, by replacing a section of the upper skin of the wing with a series of angled slats. He believed that this would produce superior lift and stability compared to typical wing designs. Unfortunately, only very limited information relating to the practical implementation of Lanier's designs, that are now ninety years old, can be found. The patents by their nature are legal rather than scientific documents. A few nontechnical articles appeared around the time of the patents in contemporary popular science magazines [5, 6, 23], where the aircraft was described as a "vacuplane" [5]. A more recent discussion paper was presented at the MODSIM 2013 conference [11]. However, to this day, we are unable to find any scientific examination of the designs in the literature aside from our MISG report.

We start in Section 2 with a brief overview of aerodynamic theory and give some historical context to Lanier's ideas in the history of flight. In Section 3, we review the patents and glean some sparse relevant information from them. In Section 4, we first

https://doi.org/10.1017/S1446181123000068 Published online by Cambridge University Press

infer lift from the performance of the vacuplane as claimed in the existing documents, and then compare this with lift calculated using an inviscid-flow model. In Section 5, we compare results of viscous-flow simulations, performed with the finite-element PDE solver *Fastflo* [7], for a "slat-wing" airfoil (with open top surface) and a more conventional closed airfoil. We also use numerical simulations from the *Fastflo* PDE solver to study viscous flow over a single slot. Conclusions are given in Section 6.

2. Background theory and historical perspective

The flight characteristics of an aircraft are determined by four different forces: lift, weight, thrust and drag. Lift and gravitational forces are in the vertical direction and must balance one another for level flight. Similarly, in the horizontal direction, the forward thrust and drag act in opposite directions and must cancel each other when the aircraft is moving at a constant speed. Lift and drag are influenced by the aerodynamics of the plane's lifting surfaces and fuselage and, consequently, are the main focus of this work. The weight is characteristic of the aircraft with its load, and thrust depends upon the engine. More detailed discussion of the following theory is found elsewhere [2, 12].

The lift and drag properties of an airfoil are usually recorded using the nondimensional lift and drag coefficients, C_L and C_D, respectively. With these, the lift on the wing

$$L = C_L \rho U^2 A/2 \tag{2.1}$$

and, similarly, the drag

$$D = C_D \rho U^2 A/2, \tag{2.2}$$

where U is the speed, A = chord × span is the projected area of the lifting surface and ρ is the air density.

Lift is generated by a difference in airflow velocity above and below a wing. The air flows more rapidly over the upper surface, and therefore has lower pressure (according to the Bernoulli equation) than the more slowly moving air under the wing. Factors influencing lift are the shape of the wing, the angle of attack and the proximity to the ground. Drag consists of two types, form and induced. Form drag is the effect of viscosity as the air "sticks" to the surface of the plane. Induced drag results from the fact that wings have a finite length; the flow of air around the wing tips, from the high-pressure region below the wing to the low-pressure region above it, creates trailing vortices that result in further drag.

Flight is a trade-off between lift and drag. Mechanisms that increase lift, such as additional flaps or small extra airfoils that prevent separation around the leading edge, usually have the effect of increasing drag. Modern aircraft usually have some of these additional devices that extend during take-off and landing where higher lift is desirable and where extra drag is less important or even is desirable as during landing.

Lift is generally proportional to the angle α of the wing relative to the direction of travel or air flow (the angle of attack) and the square of the velocity. If we assume

https://doi.org/10.1017/S1446181123000068 Published online by Cambridge University Press

that the wing span S is long relative to its thickness and chord (breadth), then the flow is essentially two-dimensional enabling us to consider flow in a plane containing a cross-section of the wing; the term "airfoil" denotes the cross-sectional profile of a wing. Lift per unit wing-span can then be quantified by the formula $\ell = L/S = \rho U\Gamma$, where the circulation $\Gamma = \oint \mathbf{q} \cdot \mathbf{dr}$, which is the integral of the flow velocity $\mathbf{q}$ around a loop containing the wing cross-section. This has to be determined subject to the Kutta condition; that the air flow separates smoothly from the (sharp) trailing edge of the wing/airfoil. For relatively thin, symmetric wings, $\Gamma \approx \pi UC \sin\alpha$, where C is the chord length of the wing/airfoil, so that the lift per unit span is $\ell = \pi\rho U^2 C \sin\alpha$, or $C_L = 2\pi \sin\alpha$.

However, if the angle of attack becomes too large, the flow no longer follows around the airfoil, but separates from the upper surface leading to a sudden and dramatic loss of lift called *stall*. A thicker airfoil means a greater likelihood that stall will occur since the air has to divert more rapidly around the blunter leading edge, but it can also be influenced by the roughness of the surface, and in older aircraft, especially in the early metallic bodies, this could play a significant role.

Aircraft from the time of the Wright Brothers until after World War I were mostly bi-planar. Biplanes typically had two thin wings made of wood and canvas held together by a variety of struts and wires. These were relatively light and so required less lift, but had high drag due to the wires, struts and rough surfaces. There was, however, significant loss of aircraft and pilots during World War I due to leading-edge stall at sufficiently large angle of attack, and consequent aeroplane spin. This motivated the development (~1917–1929) by Sir Frederick Handley Page and Dr Gustave Lachmann, at first independently and then in cooperation, of a slot along the leading edge of the wing, formed by placing a slat ahead of the front edge of the main wing. Thus, the leading edge of the slat formed the leading edge of the wing as a whole, and the slot between the slat and the main wing allowed air flow from the bottom to the top of the wing in such a way as to prevent leading-edge stall [9]. The year 1927 saw the development of a moving slat that operated automatically with aerodynamic forces to close the slot at low angle of attack (reducing drag) and open it at higher angle of attack when needed to prevent stall. As reported by Green [9], "In the assessment of C. G. Grey, founder and first editor of *The Aeroplane* magazine, the importance of the slot to aeronautics was similar to that of the pneumatic tyre to the motor car." The increase in lift and reduction in the lift-to-drag ratio is shown in [1, pp. 227–229].

Lanier's work seems to have started just as the leading-edge slot and accompanying slat were being refined and, like that of Page and Lachmann, appears to have been aimed at increasing lift and improving aircraft safety. By the 1930s, however, monoplanes were becoming the dominant form of aircraft. Early monoplane wings were still quite thin, although they were thicker than biplane wings because the structural framework was internal. The slightly thicker wings generated slightly higher lift, but more powerful engines enabling higher speeds and hence considerably more lift (increasing with the square of speed) were a major factor in enabling the evolution of the monoplane. Leading-edge stall was not a feature of these thicker wings and

attention was turned to slotted flap design and laminar flow control to reduce drag [9]. Rapid development between the two World Wars led to planes designed for both long distance travel and high air speed, as adventurers tried to set records of both types. Further rapid advances in aircraft design during World War II led to the first jet-powered craft. Interestingly, swept-wing jet aircraft brought back the possibility of tip stall and the use of slatted wings with a leading-edge slot [9].

3. Lanier's patents

Lanier's six US patents for aeroplanes from the early 1930s [13–18] each cover several aspects of an entire aircraft design rather than focussing on a specific feature. In this paper, we are specifically interested in the presence of cavities or slats on the upper surface of the wing and fuselage. The early patents claim that the cavity designs improved stability while later patents further claim enhanced lift.

The patents attempt to explain increased lift from one or more cavities in the wings and/or fuselage as an effect of a partial vacuum set up in the aeroplane's wings and body. This space would then be at a lower density than the air surrounding the aircraft, increasing buoyancy. An additional lift effect is anticipated by exposing the inside top surface of the lower shell of the wing. As patents, the descriptions tend to be rather general without detailed measurements.

The idea of a "vacuum chamber" is introduced in the first two patents from 1930. The removal of a portion of the upper wing surface allows flow between the internal wing cavity and the exterior. The proposed function is improved stability [13]:

> *. . .it is an object to provide a machine that will not nose dive, side slip or tail spin under ordinary circumstances, but should this happen, the machine will right itself without the pilot aid.*

The second patent is directed towards larger aircraft. It includes the idea of a system of slats (or air buffers) across the hole in the upper wing surface with the purpose of reducing airflow into the vacuum chamber [14]:

> *When the plane is moving at slow speed or the engine is throttled down, there is a tendency for the air to flow down into the vacuum chamber from above. The provision of the air buffers, however, causes this air to be deflected upwardly and rearwardly, thus preventing it from entering the vacuum chamber to any considerable extent.*

These buffers would not extend to the base of the vacuum chamber and would preferably be hinged so that they could close the top of the vacuum chamber when desired. The buffers remained a feature of the later patents and in the fourth patent, there is the further claim of increased lift [16]:

> *I have found by experiments and tests that the lifting power of the vacuum chamber exceeded my expectations, and I have further found that an aeroplane*

https://doi.org/10.1017/S1446181123000068 Published online by Cambridge University Press

can be designed utilising the principle of the vacuum chamber lift in which the wings can be wholly eliminated or reduced to dwarf wings, . . .

The fifth patent [17] contains many of the earlier features and claims, and is perhaps the most useful for obtaining an insight into the inventor's thoughts. As well as reiterating the goal of safety through stability, it mentions features that would be associated with a reduced wing size and increased lift. The vacuum chamber here extends to the whole of the wing and perhaps a portion of the fuselage. There is an explicit claim that the partial evacuation of air leads to an increased lift. In addition to this lift, due to the buoyancy of a reduced air density within the plane (as in a balloon), the inventor also appears to claim a mechanical lift by exposing the bottom inner surface of the wing (in practice, this would in part be offset by reduced lift on the inner top surface of the wing). He states that apart from the vacuum pocket, the wings can be otherwise conventional:

The theory of getting additional lift from a given wing area is applicable to the conventional wings of today with few changes, simply by making the wing air-tight and supplying vents or openings in the top surface to evacuate the air, thus increasing the payload without an increase in structural weight. Lift is also exerted on the inside bottom skin of the airfoil above the cabin which, on the conventional wing, is negligible. On planes with large cabins this additional lift would greatly increase payload.

4. Lift calculations

4.1. Inferences from performance claims In horizontal flight, the lift must balance the weight of the aircraft. Therefore, we can estimate the lift coefficient for the aircraft described in Lanier's patents by considering the weight.

The Lanier Vacuplane of 1935 had a gross weight (including the pilot) of 574 pounds ($M = 260$ kg), a take-off/landing speed as low as 30 mph (≈ 48 km/h or 13.3 m/s), a cruising speed for level flight of 80 mph ($U = 128$ km/hr ≈ 35.6 m/s) and a wing area of 73 square feet ($A \approx 7$ m^2) [4]. Using the density of air $\rho = 1.23$ kg/m^3 at 15°C and atmospheric pressure, the lift equation (2.1) gives a lift coefficient $C_L \approx 2Mg/(\rho U^2 A) \approx 0.47$, where $g = 9.8$ m/s^2 is the acceleration due to gravity. This is comparable with lift coefficients of conventional aircraft.

The Lanier Paraplane Commuter 110 (see [4]) was built by Lanier aircraft corporation around 1949, 16 years after the original patents were submitted, and is of unknown design. This aeroplane had similar take-off and cruise speeds but a greater mass (640 kg), and roughly 30% greater wing area, giving a lift coefficient of $C_L \approx 0.88$, again within conventional values.

Further to this, we can estimate the drag coefficient by considering the maximum speed. The 1935 Vacuplane [4, 19] had a 36 horsepower engine ($P_E \approx 27$ kW), and an estimated top speed of 96 mph (≈ 154 km/h or 43 m/s). Drag $D = C_D \rho U^2 A/2$ (2.2)

https://doi.org/10.1017/S1446181123000068 Published online by Cambridge University Press

and the power required to overcome this drag is $P = DU \approx 3.4 \times 10^5 C_D$ Watts, so $P \approx 340 C_D$ kW. By comparison, we see that the drag coefficient is $C_D \approx 0.079$.

The Lanier Paraplane Commuter 110 had a maximum speed of 165 mph ($\approx$ 74 m/s), a 150 Hp $\approx$ 112 kW engine and a slightly greater wing area. Using the same approach, $P \approx 2300 C_D$ kW, and therefore the drag coefficient $C_D \approx 0.049$.

Subsequent calculations use an airfoil shape approximating the Clark-Y wing [12]. For comparison, the lift and drag coefficients of this wing at 0° (6°) angle of attack are $C_L = 0.36$ (0.80) and $C_D = 0.0217$ (0.045).

These basic calculations are built on less than ideal data extracted from popular literature. Nevertheless, they indicate that there is nothing extraordinary in the behaviour of the Lanier aircraft.

A further implication in some of the popular literature and Lanier's patents (see Section 3) is that there is a buoyancy effect of air being sucked out of the wing cavity. However, it is easy to show that the effect of reducing air density within the wings would have an almost negligible effect, perhaps lightening the aeroplane by a few hundred grams. For example, the total weight of air in a wing cavity with a volume of two cubic metres (estimated for the Lanier XL-4) is approximately 2.4 kilograms or approximately 1% of the total weight. However, since not all of the air could be evacuated, this is a very generous upper bound. In heavier, larger craft, this proportion would be greatly reduced.

In a stall situation, the pressure would equalise between the inside and outside of the wing, causing the air to rush back in, negating any buoyancy effect in free flight. It may be that the effect of drag on the lighter and slatted (and hence rougher) wings is greater than that on the engine and cabin, causing the plane to right itself as it falls, but this will depend on the plane's attitude at stall.

4.2. Inviscid theory for an elliptic airfoil In this section, we assume a large wing span relative to its chord length so that we may solve for the two-dimensional flow about the cross-section of the wing. We also assume an elliptic cross-section and, hence, compute the lift on an elliptic airfoil, the centre of which is at height H above the ground, using an integral equation method to determine the effects of wing thickness, angle of attack and proximity to the ground. The lift on an airfoil can be determined by inviscid flow theory with the ground effect included using the method of images, that is, we consider the flow around the ellipse and its image such that the ground is a line of symmetry between the two. Assuming an inviscid, incompressible fluid, the flow is irrotational so that the problem reduces to that of solving for the velocity potential Φ, where the velocity field $\mathbf{q} = \nabla\Phi$, and Φ must satisfy Laplace's equation $\nabla^2\Phi = 0$.

One way to do this is to compute the complex potential $w(z) = \Phi + i\Psi$, where $z = x + iy$, y being vertical distance above the ground and Ψ is the streamfunction. For our problem, the complex potential is given by

$$w(z) = Uz + \frac{i\Gamma}{2\pi}\log(z^2 + H^2) + \chi(z), \tag{4.1}$$

https://doi.org/10.1017/S1446181123000068 Published online by Cambridge University Press

where the first term represents the free stream flow with velocity U, the second the circulation around the airfoil and the third, $\chi(z)$, is to be determined to satisfy the boundary conditions for the flow. From complex function theory, we have that the velocity potential Φ satisfies Laplace's equation provided $w(z)$ is an analytic function. The streamfunction Ψ must be constant on the surface of the airfoil so that there is no flow through the surface of the airfoil, that is, $\mathbf{q} \cdot \mathbf{n} = 0$, where $\mathbf{n}$ is the normal to the boundary of the airfoil which has upper and lower surfaces $y = f^{\pm}(x)$. Similarly, Ψ is constant on the ground $z = x + i0$.

Using Cauchy's integral formula to integrate the function $\chi(z) = \xi + i\eta$ around a contour including the airfoil, its image on reflection in the line of symmetry of the ground and a circle of infinite limiting radius leaves

$$\chi(z_0) = \frac{1}{2\pi i} \int_\gamma \frac{\chi(z)}{z - z_0}\, dz,$$

where γ consists of that part of the contour around the surface of the airfoil and its image. Defining arclength s, where $ds = \sqrt{dx^2 + dy^2}$, and using the chain rule together with the symmetry of the airfoil and its image, it can be shown that the real part of χ, that is, ξ, is given by the integral equation

$$\xi(s) = \frac{1}{\pi} \int_0^{s_L} \frac{\xi(t)[y'(t)\Delta x - x'(t)\Delta y] - \eta(t)[x'(t)\Delta x + y'(t)\Delta y]}{(\Delta x^2 + \Delta y^2)} + \frac{\xi(t)[y'(t)\Delta x - x'(t)\Delta y_+] - \eta(t)[x'(t)\Delta x + y'(t)\Delta y_+]}{(\Delta x^2 + \Delta y_+^2)}\, dt, \tag{4.2}$$

where s_L is the arclength from the trailing edge of the body to the leading edge then back, $\Delta x = x(t) - x(s)$, $\Delta y = y(t) - y(s)$ and $\Delta y_+ = y(t) + y(s)$.

Thus, the method is to write the surface of the airfoil in parametric form $(x(s), y(s))$, and then take a discrete form of the integral using steps in arclength, s_k, $k = 1, 2, \ldots, N$. Replacing the integral by a sum, the unknown $\xi_k = \xi(s_k)$ can be obtained by solving N equations in N unknowns. Further details of the method can be found in [20].

We also know from (4.1) that the function $\chi(z) = \xi + i\eta$ is made up of the following components:

$$\xi(s) = \Phi(s) - Ux(s) + \frac{\Gamma}{2\pi}(\beta_1(s) - \beta_2(s)),$$
$$\eta(s) = \Psi_0 - Uy(s) - \frac{\Gamma}{2\pi} \ln\left[\frac{\rho_1(s)}{\rho_2(s)}\right],$$

where Ψ_0 is the (constant) value of the streamfunction on the airfoil surface,

$$\rho_1 = (x^2 + (y - H)^2)^{1/2}, \quad \rho_2 = (x^2 + (y + H)^2)^{1/2}$$

are the distances between $z = \pm iH$ and points $z = x(s) + iy(s)$ on the surface, and

$$\beta_1 = \arctan\left(\frac{y - H}{x}\right), \quad \beta_2 = \arctan\left(\frac{y + H}{x}\right)$$

https://doi.org/10.1017/S1446181123000068 Published online by Cambridge University Press

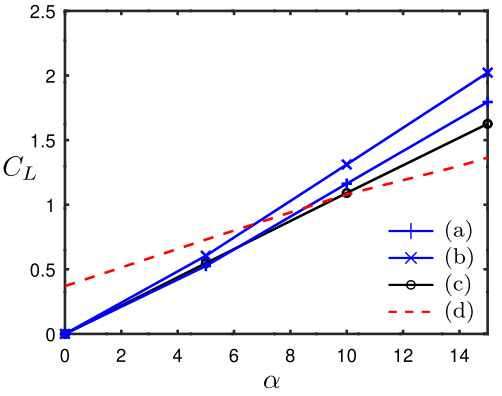

FIGURE 1. Lift coefficient C_L versus angle of attack α for elliptic airfoils of (dimensionless) thickness (a) $\tau = 0.1$ and (b) $\tau = 0.2$. Also shown for comparison is C_L versus α for (c) a flat plate as given by the analytic formula, and (d) a Clark-Y wing having $\tau \approx 0.12$ for which stall occurs at $\alpha \approx 18.5°$.

are the angles of lines between $z = \pm iH$ and points on the surface. Thus, η is known everywhere on the surface, and the integral equation (4.2) can be used to find ξ and hence the velocity potential.

The crucial factor in determining the lift is the Kutta condition, which requires that the flow detaches smoothly from the end of the airfoil. The circulation Γ must be chosen to ensure this condition is satisfied. This was achieved by allowing Γ to be one of the unknowns and including an extra equation to enforce this condition. In the case of an ellipse having a blunt end, it was required that the stagnation point forms at the trailing edge (i.e. rear-most point) of the ellipse.

A `Fortran` program was written to implement this solution method and simulations were performed using this code for various values of wing chord, thickness, angle of attack and height above the ground. Figure 1 shows an increase in the theoretical lift C_L with increasing angle of attack α for elliptic airfoils at large height ($H \to \infty$) above the ground (no ground effect) with maximum dimensionless thickness $\tau = 0.1, 0.2$ (scaled with chord-length C). These data are compared with the lift on a flat plate (or thin symmetric airfoil), computed using the analytic formula $C_L = 2\pi \sin\alpha$, and with the lift coefficient for the Clark-Y wing which has $\tau \approx 0.12$. Clearly, the nonsymmetric Clark-Y airfoil performs much better at small angle of attack than those used for numerical experiments. Moreover, its lift coefficient continues to increase through to $\alpha \approx 18.5°$ beyond which it will stall (lose lift). In contrast, the other airfoils will undergo stall at much lower angles of attack, which is not apparent from the figure because separation and stall were not computed. The effect of wing thickness is seen for the elliptic airfoil; doubling τ from 0.1 to 0.2 increases the lift by approximately 10% at each angle of attack.

Figure 2 shows the effect of proximity to the ground $h = H/C$ on the lift coefficient for airfoils of several different values of (dimensionless) thickness τ. It is clear that

https://doi.org/10.1017/S1446181123000068 Published online by Cambridge University Press

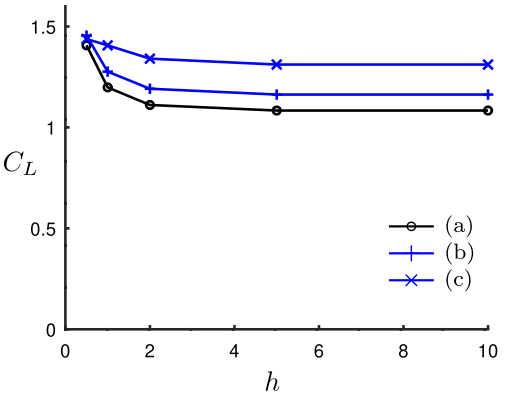

FIGURE 2. Lift coefficient C_L versus (dimensionless) height $h = H/C$ above ground for elliptic airfoils of (dimensionless) thickness (a) $\tau = 0.05$, (b) $\tau = 0.1$ and (c) $\tau = 0.2$, all at angle of attack $\alpha = 10°$.

ground effect increases lift when the ground is within one or two chord-lengths C of the airfoil, suggesting that ground effect can be neglected from our deliberations.

In general, wing profile designs must balance lift with drag. Our results confirm that thicker wings tend to give greater lift for a given speed. However, they also tend to have increased drag making it more difficult to attain speed. In addition, thicker wings at higher speed are more likely to induce separation of the flow and, hence, stall.

At the time of Lanier's patents, wings were generally narrow in profile. However, one of his patents includes an illustration of a conventional wing together with the slatted wing of the patent design [18]. The slatted wing is drawn much thicker than the conventional wing and if this was the case in practice, then this might explain an increase in lift for the Lanier aeroplane. Note, however, that the simple calculations in the previous section suggest that the lift of the Lanier craft was not exceptional compared to conventional airfoils such as the Clark-Y wing.

5. Viscous flow simulations

To investigate viscous effects, a limited numerical exploration was conducted using the finite-element package *Fastflo* [7], as described below.

5.1. Two-dimensional viscous flow over an airfoil The form drag of an airfoil is due to the viscosity of the fluid and to determine this, as well as its lift, we cannot use inviscid theory. Here, we consider two-dimensional viscous flow around thick and thin airfoils, with and without Lanier-type cavities, at different angles of attack. We necessarily neglect induced drag, which is a three-dimensional effect as described earlier, although this can be significant, especially for short wings. We have also made no attempt to compute form drag from the aircraft fuselage, focusing rather on the trade-off between lift and drag for a "slat-wing" airfoil compared to a conventional airfoil.

https://doi.org/10.1017/S1446181123000068 Published online by Cambridge University Press

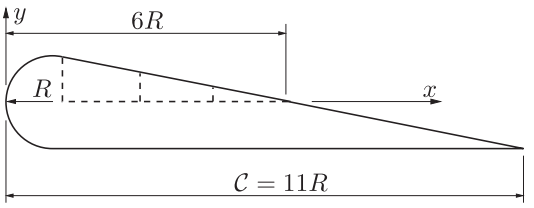

FIGURE 3. Typical "thick" airfoil geometry. Conventional airfoil shown solid; cavity and vertical slats shown dashed. (Reproduced from [10].)

The geometries of the thick airfoils used in the simulations are shown in Figure 3. The basic airfoil shape superficially resembles the Clark-Y wing [12]. The chord length C of the airfoil is eleven times the nose radius R. For comparison with the conventional shape, the flow around a similar shape with a cut away cavity and slats, to resemble the Lanier "slat-wing" design, is also considered. The thin airfoil geometries are obtained by halving lengths in the vertical direction, giving a less blunt elliptical nose. Again, a conventional closed airfoil and a "slat-wing" geometry are considered.

The flow is assumed to be two-dimensional, incompressible, steady and laminar, with a Reynolds number of 10. Although, Reynolds numbers of order 10^5 are to be expected, this was about the maximum that *Fastflo* could reliably handle. Further, the flow would almost certainly be turbulent, but only laminar flow was considered. Despite these drawbacks, the simulations still allow a comparison of the fundamental behaviour of a conventional airfoil and a Lanier "slat-wing" airfoil. Separation of the flow from the airfoil is expected to occur at lower angles of attack for the blunt-nosed thick airfoil than for the thin airfoil.

The continuity and steady Navier–Stokes equations must be solved for the flow around four different airfoils (thick/thin × conventional/"slat-wing"), subject to no-slip on the airfoil boundary. A reference frame is adopted that moves with the airfoil at speed U. The horizontal and vertical axes are x and y, respectively, with the origin at the tip of the nose of the airfoil (see Figure 3). Let u, v be the x, y components of velocity scaled with U, and let p denote pressure scaled with ρU^2. Lengths are scaled with the nose radius R. Then the dimensionless continuity equation is

$$\frac{\partial u}{\partial x} + \frac{\partial v}{\partial y} = 0, \tag{5.1}$$

and the Navier–Stokes equations are

$$u\frac{\partial u}{\partial x} + v\frac{\partial u}{\partial y} = -\frac{\partial p}{\partial x} + \frac{1}{Re}\left(\frac{\partial^2 u}{\partial x^2} + \frac{\partial^2 u}{\partial y^2}\right), \tag{5.2}$$

$$u\frac{\partial v}{\partial x} + v\frac{\partial v}{\partial y} = -\frac{\partial p}{\partial y} + \frac{1}{Re}\left(\frac{\partial^2 v}{\partial x^2} + \frac{\partial^2 v}{\partial y^2}\right), \tag{5.3}$$

https://doi.org/10.1017/S1446181123000068 Published online by Cambridge University Press

where $Re = UR/\nu$ is the Reynolds number, ν being the kinematic viscosity of air ($\approx 1.5 \times 10^{-5}$ m^2/s). On the boundary of the airfoil, we have $u = v = 0$. Far upstream of the airfoil, the flow is taken to be a uniform stream of magnitude U at angle of attack α. Sufficiently far above and below the airfoil, we expect the flow to be that of a uniform stream also. As the solution must be done over a finite computational domain, a square far-field boundary is defined with sides of length $20R$ around the airfoil, aligned with the far-upstream flow and with centre at the tip of the nose of the airfoil $(x, y) = (0, 0)$. Thus, on the inlet (left), top and bottom boundaries, the velocity is specified as $u = \cos\alpha$, $v = \sin\alpha$. The outlet (right) boundary is assumed to be a stress-free boundary. The far-field boundary is sufficiently far from the airfoil that the prescribed boundary conditions do not have significant impact on the solution.

The finite-element PDE solver *Fastflo* was used to solve for the flow. *Fastflo*'s automatic mesh generator was used to generate an unstructured mesh of approximately 1900 6-node triangles over the computational domain, with elements clustered more densely near the airfoil. The "augmented Lagrangian method" [7, Section 13.3] and quadratic basis functions were used to solve for pressure and velocity.

Having solved for velocity and pressure, lift and drag forces per unit wing-span were found by integrating the pressure around the surface of the airfoil $d\Omega$, that is,

$$\frac{\mathbf{F}}{\rho U^2 R} = \oint_{d\Omega} p \, d\mathbf{r}.$$

Resolving the force per unit span obtained into two components $\mathbf{F} = (F_x, F_y)$, the drag $D = F_x \cos\alpha - F_y \sin\alpha$ in the direction of the uniform stream, and the lift $L = F_x \sin\alpha + F_y \cos\alpha$ normal to it. From these, the lift and drag coefficients were computed as

$$C_L = \frac{2L}{11\rho U^2 R}, \quad C_D \approx \frac{2D}{11\rho U^2 R}.$$

Table 1 shows these coefficients for different angles of attack α for each of the four airfoils considered, while they are plotted against α in Figures 4 and 5, respectively. Figure 6 shows the ratio of lift to drag, i.e. C_L/C_D, again versus angle of attack. In Figures 7–10, we show stream lines around the airfoils and velocity vectors near the upper surface behind the nose of the airfoils.

A comparison of the curve for the Clark-Y wing in Figure 1 with those for the thin wings in Figure 4 shows the lift coefficients to be of a similar order of magnitude at the same angle of attack and gives some assurance that the general behaviour of the wings under investigation is captured by the low Reynolds number simulations. It is expected that at higher Reynolds number, the boundary layers will be thinner and the lift coefficients a little larger. In keeping with known aerodynamic behaviour, the lift coefficient for the thick wings is larger than for the thin wings at small angle of attack, however, the slope of the curve C_L versus angle of attack α is greater for thin wings than for thick wings so that this situation reverses at larger angle of attack. (For thin symmetric wings, $C_L/\sin\alpha \sim 2\pi$, while $C_L/\sin\alpha \sim 4$ for the thin asymmetric airfoils considered

https://doi.org/10.1017/S1446181123000068 Published online by Cambridge University Press

TABLE 1. Lift (C_L) and drag (C_D) coefficients at angle of attack α for thick and thin conventional and "slat-wing" airfoils. (Reproduced from [10].)

α	Coefficient	Conventional		"Slat-wing"	
		Thick	Thin	Thick	Thin
0	C_L	0.31	0.18	0.31	0.21
	C_D	0.21	0.11	0.24	0.13
5	C_L	0.54	0.54	0.53	0.55
	C_D	0.26	0.15	0.28	0.16
10	C_L	0.71	0.81	0.69	0.80
	C_D	0.33	0.23	0.35	0.23
15	C_L	0.83	1.04	0.82	1.05
	C_D	0.42	0.39	0.44	0.38
20	C_L	0.97	1.10	0.96	1.07
	C_D	0.54	0.46	0.55	0.45

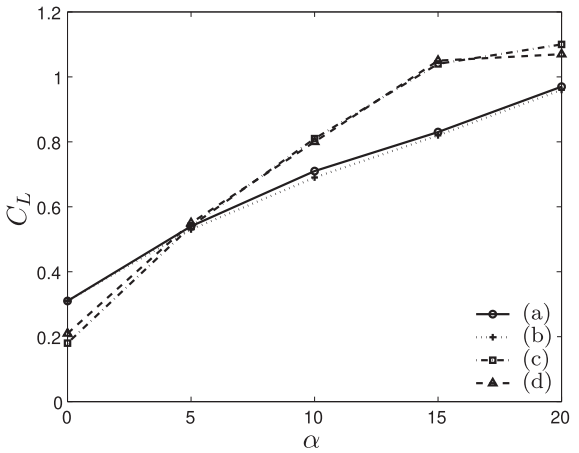

FIGURE 4. Lift coefficient C_L versus angle of attack α for the (a) thick conventional, (b) thick "slat-wing", (c) thin conventional and (d) thin "slat-wing" airfoils. (Reproduced from [10].)

here.) For the thin wings, there is a sudden decrease in slope beyond $\alpha = 15°$ signalling imminent stall (loss of lift). This is due to flow separation which occurs at approximately $\alpha = 15°$, as seen in the plots of streamlines and velocity vectors given in Figures 9 and 10. The thicker wings experience flow separation at a lower angle of attack $\alpha \sim 10°$, as seen in Figures 7 and 8, but do not exhibit such a sudden reduction in lift. It is readily seen that the conventional airfoil and corresponding "slat-wing" airfoil, whether thick or thin, differ little from one another in terms of lift coefficient.

https://doi.org/10.1017/S1446181123000068 Published online by Cambridge University Press

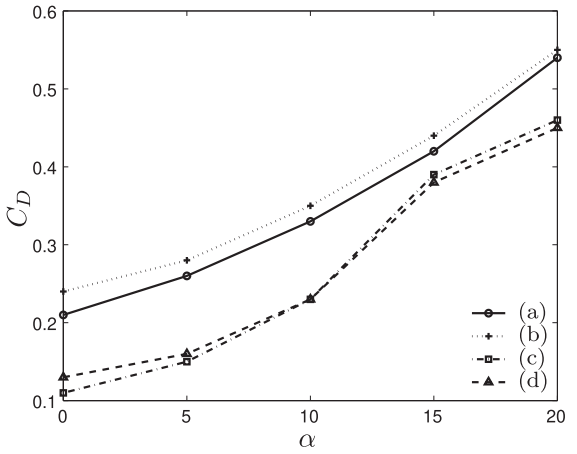

FIGURE 5. Drag coefficient C_D versus angle of attack α for the (a) thick conventional, (b) thick "slat-wing", (c) thin conventional and (d) thin "slat-wing" airfoils. (Reproduced from [10].)

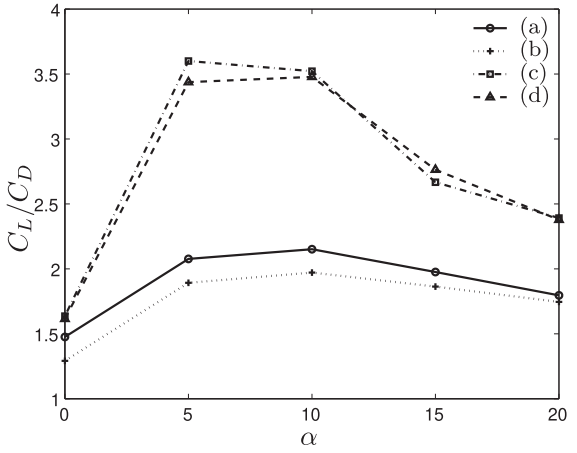

FIGURE 6. Ratio of lift to drag C_L/C_D versus angle of attack α for the (a) thick conventional, (b) thick "slat-wing", (c) thin conventional and (d) thin "slat-wing" airfoils. (Reproduced from [10].)

As is to be expected, the drag coefficient increases with angle of attack, as seen for all airfoils in Figure 5. For the thin airfoils, we have $C_D \approx 0.1$ (0.15) at $\alpha = 0°$ (5°) compared with $C_D \approx 0.022$ (0.045) for the Clark-Y wing. It is expected that with thinner boundary layers at higher Reynolds numbers, drag coefficients will be lower than indicated by our simulations. There is a significant increase in drag for the thin airfoils from $\alpha = 10°$ to $\alpha = 15°$, which may be attributable to a relatively large increase in the projection of the surface area normal to the flow, an effect which would be smaller for thicker airfoils. There appears to be a slight increase in drag for the

https://doi.org/10.1017/S1446181123000068 Published online by Cambridge University Press

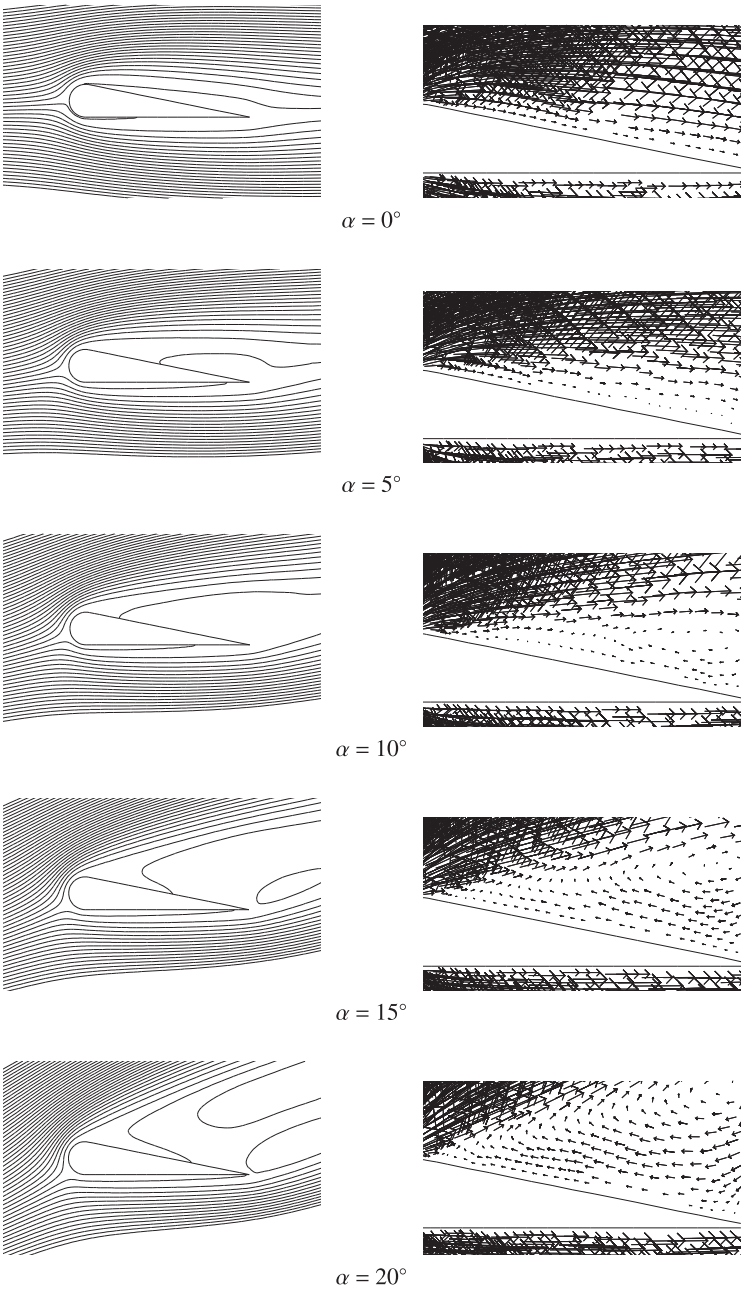

FIGURE 7. Thick, conventional airfoil. Streamlines and velocity vectors. (Reproduced from [10].)

https://doi.org/10.1017/S1446181123000068 Published online by Cambridge University Press

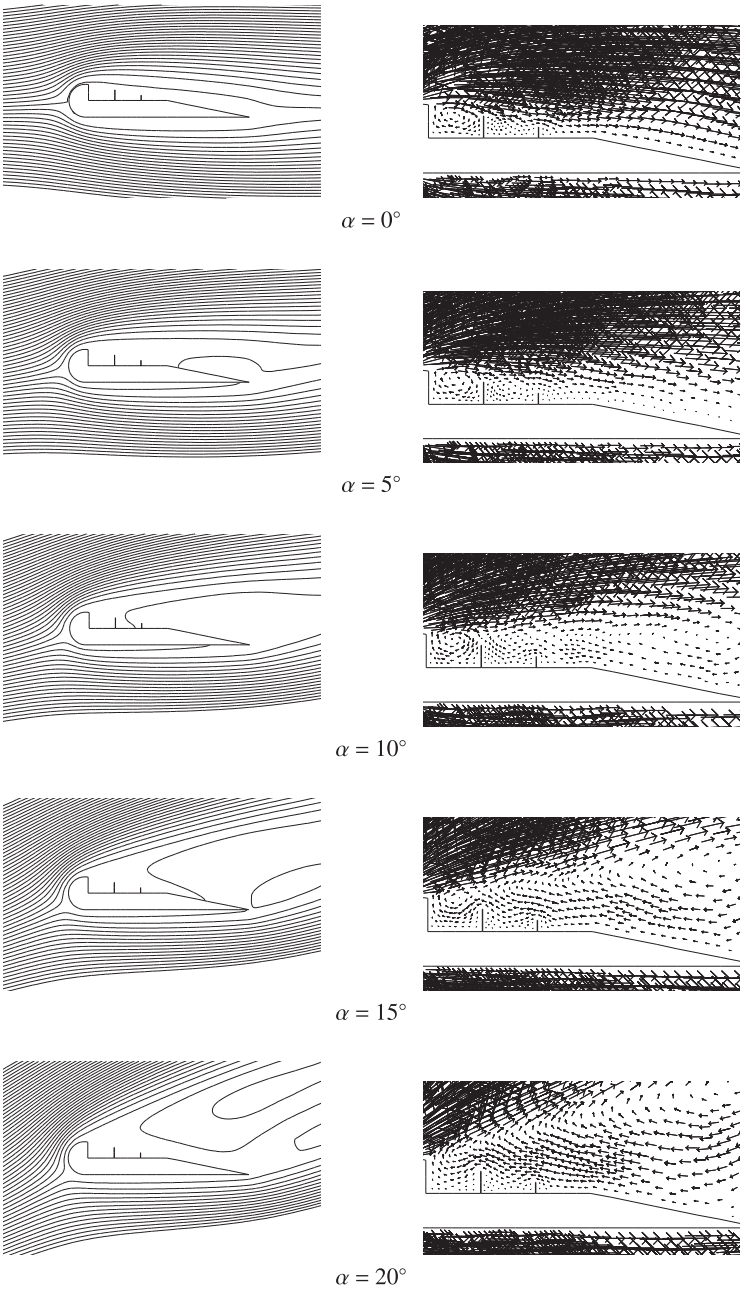

FIGURE 8. Thick, "slat-wing" airfoil. Streamlines and velocity vectors. (Reproduced from [10].)

https://doi.org/10.1017/S1446181123000068 Published online by Cambridge University Press

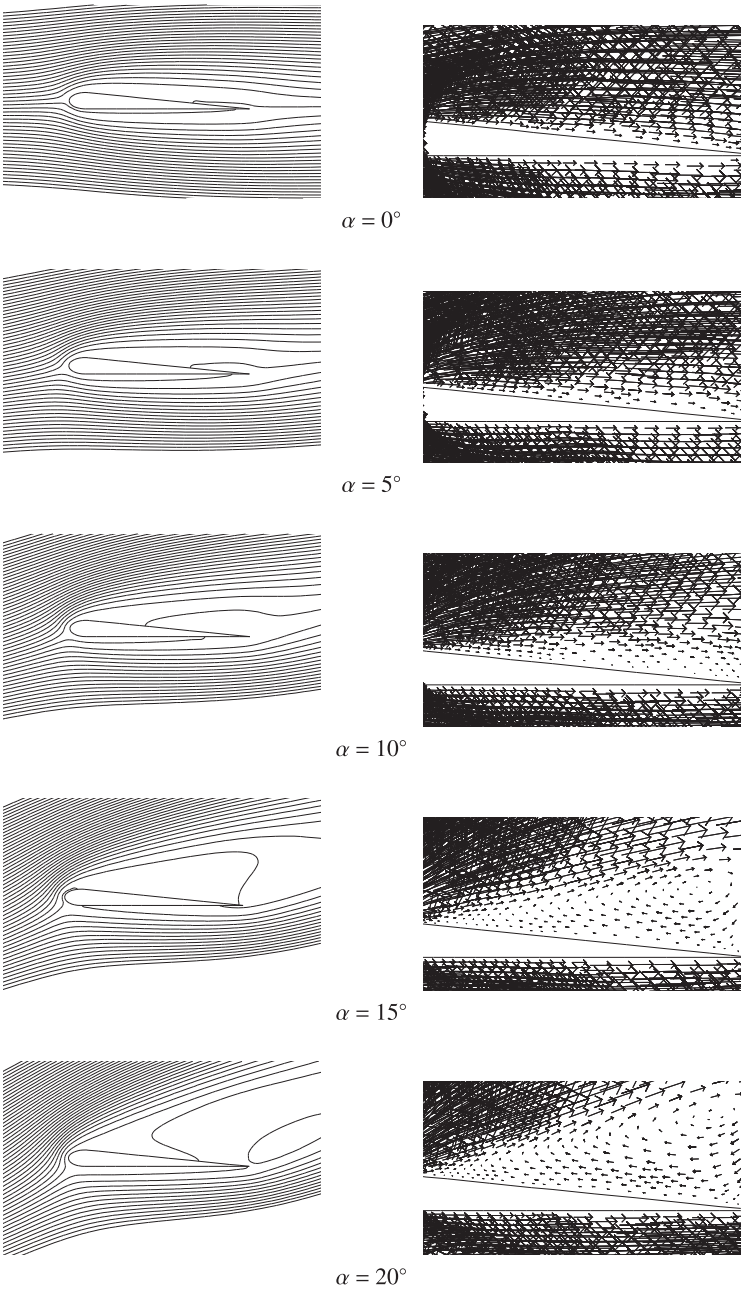

FIGURE 9. Thin, conventional airfoil. Streamlines and velocity vectors. (Reproduced from [10].)

https://doi.org/10.1017/S1446181123000068 Published online by Cambridge University Press

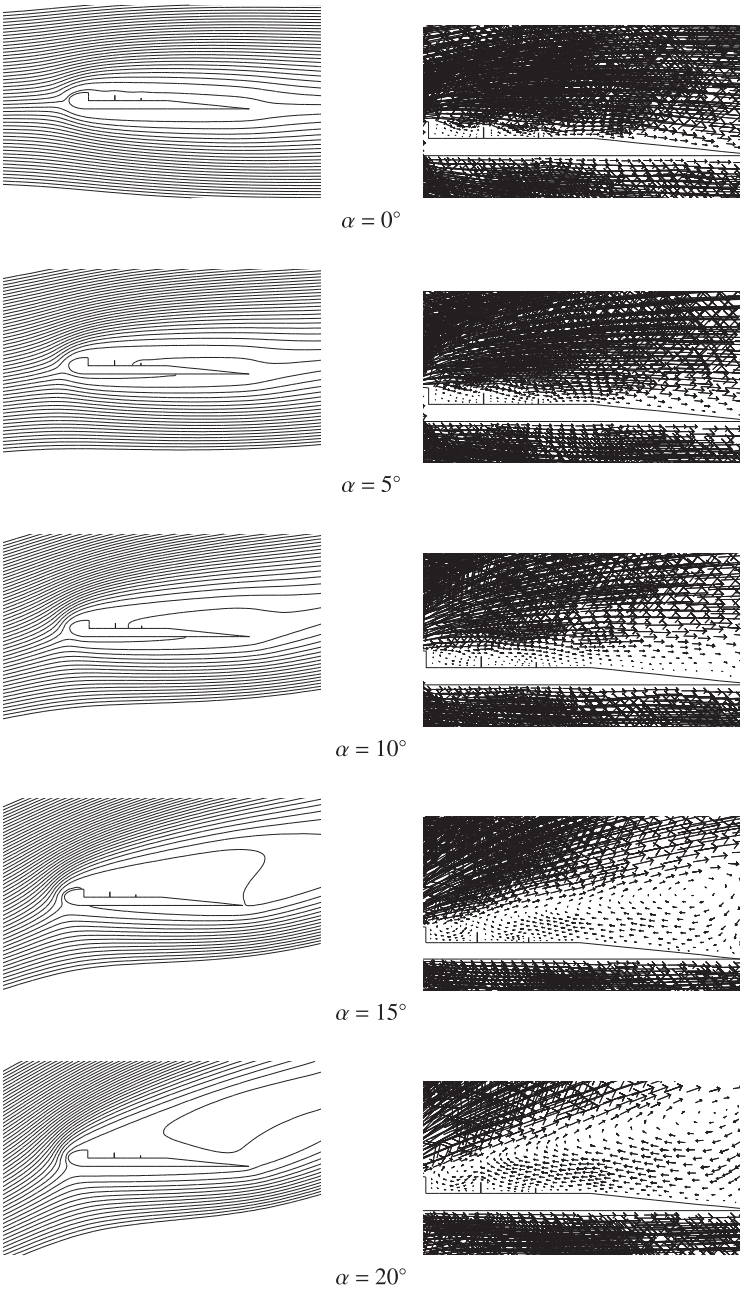

FIGURE 10. Thin, "slat-wing" airfoil. Streamlines and velocity vectors. (Reproduced from [10].)

https://doi.org/10.1017/S1446181123000068 Published online by Cambridge University Press

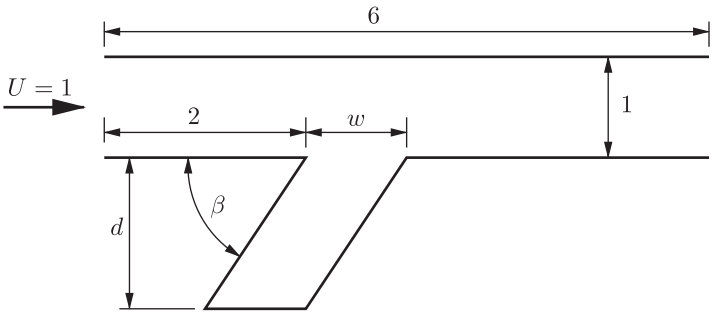

FIGURE 11. Geometry used for simulations of flow over a slot cavity. The slot aspect ratio is defined as $\varrho = w/d$. (Reproduced from [10].)

thick "slat-wing" airfoil compared to the thick conventional airfoil, but the curves of C_D versus α differ little between the two thin airfoils.

The curves of lift to drag ratio C_L/C_D versus angle of attack (Figure 6) indicate that both the thick and the thin airfoils are most efficient over the range $\alpha = 5$–$10°$. For the thick airfoils, it is evident that the conventional shape is superior to the "slat-wing" in giving slightly more lift, less drag and, consequently, a higher lift to drag ratio at a fixed angle of attack, over the full range of angles considered. For the thinner airfoils, the conventional and "slat-wing" profiles are very similar except at $\alpha = 10°$ where the conventional wing again appears to be superior.

Although we are mindful of the fact that the computations are not very accurate, the clear message emerging from our work is that our simulations certainly provide no evidence to support the "slat-wing" over conventional airfoils, but, if anything, the reverse.

5.2. Viscous flow over a slot Further numerical simulations were done to illustrate the general features of flow over a slot cavity. The typical dimensionless geometry used for these is shown in Figure 11. The continuity and Navier–Stokes equations (5.1)–(5.3) were solved, again using *Fastflo* and the augmented Lagrangian method with quadratic basis functions. At the inlet (left boundary), we specified the flow to be that of a unit uniform stream ($U = 1$), while the outlet (right) was defined to be a stress-free boundary. The lower boundary containing the cavity is, of course, a no-slip boundary ($u = v = 0$); at the upper boundary, we specified no normal flow ($v = 0$) and no tangential stress, that is, this is a slip boundary. A mesh of approximately 3000 6-node triangles was used over the computational domain.

The effects of slot aspect ratio ($\varrho = w/d$) and slot angle β were considered to a limited extent. Pressure contours and streamlines are shown in Figure 12 for a cavity of depth $d = 1.5$ and width $w = 1$ at angles of inclination $\beta = 60°, 90°, 120°$. These were computed at a Reynolds number of $Re = 1000$; at higher Reynolds numbers, convergence difficulties were experienced. The results shown are typical of cavities of both larger and smaller aspect ratio, although the width and depth of the slot does vary

https://doi.org/10.1017/S1446181123000068 Published online by Cambridge University Press

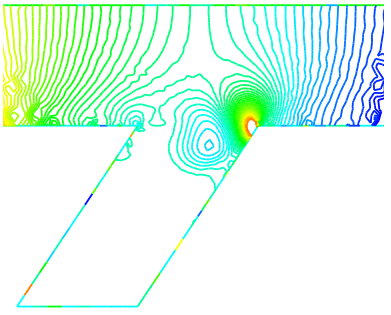

Pressure, $\beta = 60°$.

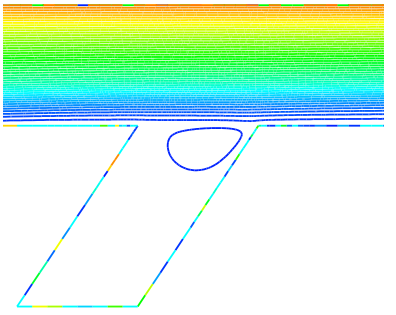

Streamlines, $\beta = 60°$.

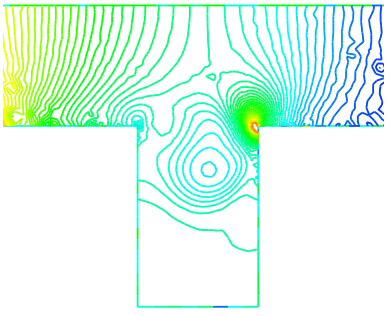

Pressure, $\beta = 90°$.

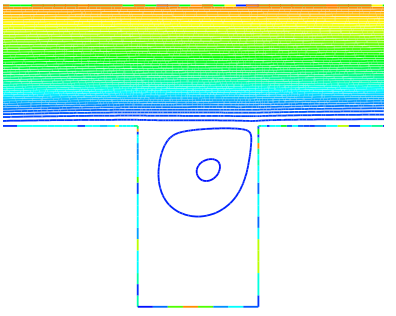

Streamlines, $\beta = 90°$.

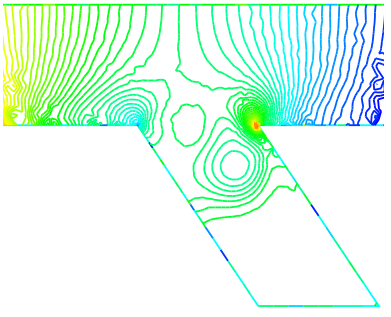

Pressure, $\beta = 120°$.

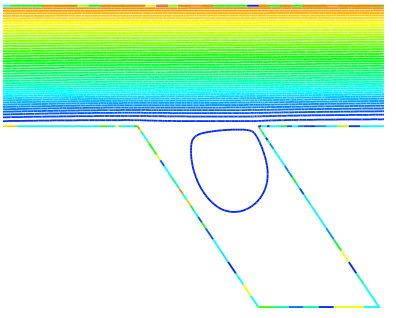

Streamlines, $\beta = 120°$.

FIGURE 12. Flow in the vicinity of a slot of aspect ratio $\varrho = 3/2$ ($d = 1.5$, $w = 1$) at various angles of inclination β. The colour of contours from blue to red indicates the change in value from lowest to highest. (Colour available online.) (Reproduced from [10].)

https://doi.org/10.1017/S1446181123000068 Published online by Cambridge University Press

the vortex flow and pressure. As can be seen, a vortex develops in the slot. The pressure at the centre of this vortex is lower than the average pressure in the surrounding fluid, but the overall pressure in the slot is very similar to that in the fluid immediately above the slot. This confirms the earlier findings that slots in the upper surface of a wing make little difference to its lifting capacity.

6. Conclusions

We have examined the Lanier "slat-wing" design for aircraft. Our focus is on how the lift and drag of the modified airfoils compare with conventional ones. We do not consider the suggestion of improved stability that is also claimed in the inventor's patents. Our study indicates that conventional airfoils are superior, or at least equivalent, to the Lanier "slat-wing" in terms of lift. We suggest that the apparent improvement in lift and/or stability reported in the popular science literature of the time, following experiments with one or two prototypes, was a result of using thicker wings than was typical at the time, so as to accommodate a "vacuum chamber" within them. As shown herein (for example, Figure 1), thicker wings generate more lift at small angles of attack compared with thin wings. Possibly, to Lanier and co-workers, thicker wings also appeared to give greater stability, due to a less sudden stall compared with thin wings. The increased top surface roughness caused by the slats would almost certainly lead to separation at lower speeds, and hence prohibit their use at higher speeds. It is almost certain that *even if* the "slat-wing" design provided some improvement on its contemporaries, it has now been superseded by modern wing designs that include variable wing shapes, leading-edge slots, auxiliary lifting surfaces and flaps that provide greatly enhanced performance, especially during take-off and landing.

Investigation of Lanier's designs could be extended. Probably the most natural approach is to compare airfoils using wind tunnel experiments. Improved numerical experiments at higher Reynold's number might also provide further illumination on the reported performance of the "slat-wing" design, and more historical research might yield more information from the 1930s to add to the largely anecdotal information currently available. The possible stability features at low speed appear to be the most promising aspect. It could be interesting to see how the Lanier design compared with contemporary aircraft of the 1930s. However, it is unlikely that any such study would have any practical impact on modern aircraft design.

Today, concerns over aircraft have shifted to their environmental impacts and the potential to mitigate this [8]. Reduction of fuel burn through reduction of drag is one important mitigation strategy. The shift to environmentally focused design was also discussed in an interesting brief history of aircraft design from around 1910 to modern times, given in a lecture by Green (FRAeS) [9] at a Royal Aeronautical Science conference in 2009, in which the development of fully laminar flow aircraft is identified as having "the greatest potential of all" for maximum drag reduction. Natural laminar

https://doi.org/10.1017/S1446181123000068 Published online by Cambridge University Press

flow control through design of wing shape and hybrid laminar flow control employing suction are also discussed as milestones towards this ultimate goal.

Acknowledgments

In addition to the authors, who were moderators for the problem at the MISG, the following people contributed to the work done during the MISG week: Syed Naeemul Ahsan, John Cogill, Bernard Ee, Ian Howells, Sam Howison, David Jenkins, Robert McKibbin, Tom Montague, Henning Rasmussen, Tony Roberts, Alfred Sneyd and Shixiao Wang. Yvonne Stokes also thanks late Professor Ernie Tuck for some useful discussion at the time of the MISG.

References

[1] I. H. Abbott and A. E. Von Doenhoff, *Theory of wing sections: including a summary of airfoil data* (Dover Publications Inc., New York, 1959).

[2] D. J. Acheson, *Elementary fluid dynamics* (Clarendon Press, Oxford, UK, 1990).

[3] A. Araújo, M. D. Bustamante, M. Cruz, R. Novakovic and V. Rottschäfer, *Handbook for running a sustainable European study group with industry*, 1st edn (Mathematics for Industry Network; European Cooperation in Science and Technology, Brussels, Belgium, 2017). https://ecmiindmath.org/wp-content/uploads/2019/07/HANDBOOK_ESGI.pdf.

[4] P. M. Bowers, *Unconventional aircraft* (TAB Books, Blue Ridge Summit, PA, 1984).

[5] R. J. Brown (ed), "Short wing vacuplane gets lifting power from suction cells", *Popular Sci. Monthly* **120**(1) (1932) p. 57. https://books.google.com.au/books?id=qR8DAAAAMBAJ&source=gbs_all_issues_r&cad=1&atm_aiy=1930#all_issues_anchor.

[6] R. J. Brown (ed), "Inventor tests new suction plane", *Popular Sci. Monthly* **126**(4) (1935) p. 27. https://books.google.com.au/books?id=qR8DAAAAMBAJ&source=gbs_all_issues_r&cad=1&atm_aiy=1930#all_issues_anchor.

[7] CSIRO, *Fastflo version 3, Tutorial Guide* (Commonwealth Scientific and Industrial Research Organisation, Australia, 1999).

[8] J. E. Green, "Air Travel – Greener by Design – Mitigating the environmental impact of aviation: opportunities and priorities", *Aeronaut. J.* **109** (2005) 361–416; doi:10.1017/S0001924000000841.

[9] J. E. Green, "Handley Page, Lachmann, flow control and future civil aircraft", in: *Classic Lecture at Handley Page Ltd: Celebrating the centenary of the first British aircraft company* (Royal Aeronautical Society Historical Group Conference, 10 September 2009). https://podbay.fm/p/aerosociety-podcast/e/1613394495 (AeroSociety Podcast, posted 15 February 2021). https://www.aerosociety.com/media/15593/raesa0352d-hp100afternoon-p-01-00-000.pdf.

[10] G. C. Hocking, Y. M. Stokes and W. L. Sweatman, "Implementing Lanier's patents for stable, safe and economical ultra-short wing Vacu- and Para-planes", in: *Proceedings of the 2005 Mathematics-In-Industry Study Group* (ed. G. C. Wake) (Massey University, New Zealand, 2005) 119–141.

[11] P. Howden, "Planning with Lanier ultra-short stable slatwings of 1920s–1970s; budget Vacu/Para-planes", in: *Proceedings of the 20th International Congress on Modelling and Simulation (Massey University, 2013)* (eds. J. Piantadosi, R. S. Anderssen and J. Boland) (Modelling and Simulation Society of Australia and New Zealand, Inc., Canberra, Australia, 2013), 733–739. www.mssanz.org.au/modsim2013/C4/howden.pdf.

[12] B. Jones, *Elements of practical aerodynamics* (Wiley and Sons, New York, 1950).

[13] E. H. Lanier, *Aeroplane, U.S. Patent no. 1,750,529* (U.S. Patent and Trademark Office, 11 March 1930). http://www.rexresearch.com/lanier/lanier.htm#usp750.

[14] E. H. Lanier, *Aeroplane, U.S. Patent no. 1,779,005* (U.S. Patent and Trademark Office, 21 October 1930). http://www.rexresearch.com/lanier/lanier.htm#usp779.

[15] E. H. Lanier, *Aeroplane, U.S. Patent no. 1,803,805* (U.S. Patent and Trademark Office, 5 May 1931). http://www.rexresearch.com/lanier/lanier.htm#usp803.

[16] E. H. Lanier, *Aeroplane, U.S. Patent no. 1,813,627* (U.S. Patent and Trademark Office, 7 July 1931). http://www.rexresearch.com/lanier/lanier.htm#usp813.

[17] E. H. Lanier, *Aeroplane, U.S. Patent no. 1,866,214* (U.S. Patent and Trademark Office, 5 July 1932). http://www.rexresearch.com/lanier/lanier.htm#usp866.

[18] E. H. Lanier, *Aeroplane, U.S. Patent no. 1,913,809* (U.S. Patent and Trademark Office, 13 June 1933). http://www.rexresearch.com/lanier/lanier.htm#usp913.

[19] Rex Research, *Edward Lanier, Para-plane//Vacu-jet.* http://www.rexresearch.com/lanier2/lanier2.htm.

[20] B. Scott, "A boundary integral method for the solution of ground effect problems", Honours Dissertation, Dept. Mathematics, University of Western Australia, 1994.

[21] W. L. Sweatman, "Mathematics-In-Industry Study Group (MISG) steel projects from Australia and New Zealand", in: *The Impact of Applications on Mathematics, Mathematics for Industry 1*, Proceedings of the Forum of Mathematics for Industry 2013 (eds. M. Wakayama, et al.) (Springer, Tokyo, 2014) 307–322; doi:10.1007/978-4-431-54907-9.

[22] W. L. Sweatman, "Mathematics-In-Industry Study Group projects from Australia and New Zealand in the past decade", in: *Interdisciplinary Topics in Applied Mathematics, Modeling and Computational Science*, Volume 117 of *Springer Proc. Math. Stat.* (eds. M. G. Cojocaru, et al.) (Springer, Switzerland, 2015) 433–438; doi:10.1007/978-3-319-12307-3.

[23] H. H. Windsor Jr (ed.), "Third-wing airplane offers greater safety", *Popular Mechanics* **55**(1) (1931) p. 41. https://books.google.com.au/books?id=reMDAAAAMBAJ&source=gbs_all_issues_r&cad=1.